Progress in Physics of Applied Materials 6 (2026), Serial Number 10, 57–68

Semnan University

Progress in Physics of Applied Materials

journal homepage: https://ppam.semnan.ac.ir/

Structural, Magnetic, and Electrical Properties of $REFe_{0.7}Cr_{0.3}O_3$ (RE= La, Pr, Nd, Sm, and Gd) Compounds

Roksana Haji, Davoud Sanavi Khoshnoud*

Faculty of Physics, Semnan University P. O. Box 35195-363, Semnan, Iran

ARTICLE INFO

Article history:
Received: 30 July 2025
Revised: 4 September 2025
Accepted: 13 September 2025
Published online: 23 September 2025

Keywords:
Orthoferrites;
Sol-gel method;
Magnetization;
Néel temperature;
Dielectric constant;
Conductivity.

ABSTRACT

In this research, crystal information, magnetic, and electrical properties of $REFe_{0.7}Cr_{0.3}O_3$ nanoparticles were investigated via X-ray diffraction data, field-emission scanning electron microscopy images, magnetic hysteresis loops and dielectric measurements, respectively. All samples were synthesized by the sol-gel method. Results related to powder X-ray diffraction indicate that all samples are single-phase and crystallize in orthorhombic symmetry with *Pbnm* space group. By varying the rare earth (RE) ions from La to Gd, the unit cell volume decreases due to the reduction in the RE ionic radius. All samples display a weak ferromagnetic behavior with low remanent magnetization and coercivity field. The Néel transition temperature of the studied samples was determined by the temperature dependence of their magnetization. Results reveal that the Néel temperature values decrease from 583 K to 498 K with decreasing ionic radius of the RE ions. The frequency dependence of the dielectric constant in all samples follows the Maxwell-Wagner polarization model. The high dielectric constant at low frequencies emphasized the polarization mechanism associated with space charges. The $LaFe_{0.7}Cr_{0.3}O_3$ sample exhibits a colossal dielectric constant in the low-frequency range at room temperature, which can be played play a significant role in miniaturizing electronic components and fabricating high-capacitance dielectric capacitors. The frequency dependence of ac conductivity indicates a small polaron hopping mechanism. To clarify the transport mechanism for of the $REFe_{0.7}Cr_{0.3}O_3$ samples, the variations of direct electrical conductivity versus temperature were studied, which revealed a semiconducting nature.

1. Introduction

In the past decade, rare-earth orthoferrites with the chemical formula $REFeO_3$ (RE = lanthanide, Sc and Y), which show the coexistence of magnetic and ferroelectric orders above room temperature, have been widely investigated due to the interesting physics and promising practical applications [1]. In particular, these compounds have a variety of applications in various areas such as gas sensors [2], catalysts [3, 4], high-speed switches [5], energy storage devices, etc [6]. The $REFeO_3$ members crystallize in a distorted orthorhombic structure with *Pbnm* space group and possess very high antiferromagnetic Néel transition temperatures in the range of 620 to 740 K [7, 8]. The antiferromagnetic behavior of these compounds in the total magnetic ordering phase depends on the existence of three RE^{3+}-O-RE^{3+}, RE^{3+}-O-Fe^{3+}, and Fe^{3+}-O-Fe^{3+} interactions [8]. However, the presence of asymmetric Dzyaloshinskii-Moriya (DM) interaction leads to weak ferromagnetic (WFM) behavior in the $REFeO_3$ system [9].

On the other hand, several studies have reported weak ferroelectric ordering and low dielectric constant for the nanoparticles of these compounds, which are some of the drawbacks of $REFeO_3$ for practical applications [10]. Hence, to overcome their limitations and to improve multifunctional features of $REFeO_3$ compounds, researchers have replaced RE and Fe-sites with various ions as a creative

* Corresponding author.
E-mail address: dskhoshnoud@semnan.ac.ir

Cite this article as:
Haji, R. and Sanavi Khoshnoud, D., 2026. Structural, Magnetic, and Electrical Properties of $REFe_{0.7}Cr_{0.3}O_3$ (RE= La, Pr, Nd, Sm, and Gd) Compounds. *Progress in Physics of Applied Materials*, *6*(1), pp.57-68. DOI: 10.22075/ppam.2025.38505.1161

solution [11, 12]. For instance, substitution of rare earth or alkaline earth ions in RE-site modifies slightly the strength of super exchange and the DM interactions via induced distortion and tilting, consequently affecting the magnetic properties of $REFeO_3$ [13-19]. However, when the Fe-site is replaced with another transition metal ion (TM) for Fe, it changes the Fe-O-Fe interaction into RE-O-Fe/TM and Fe-O-TM interactions so that this procedure can provide an additional degree of freedom for the development of multifunctional materials that are attractive from both scientific and practical points of view [20-26]. For instance, according to the Goodenough-Kanamori (G-K) rules, replacing the Cr^{3+} ion (t^3e^0) with the Fe^{3+} ion (t^2e^3) can significantly modify the magnetic properties of $REFeO_3$ compounds owing to the variation of super exchange and DM interactions [27]. As a result of this process, the variation of electronic configuration in the Fe-site can also modify other physical properties such as electrical and optical features [24]. Hence, replacement of Fe^{3+}cations in $REFeO_3$ compounds with Cr^{3+} ions has widely provided a lot of interest in recent years [28-31]. As can be seen from the literature, less attention has been paid on physical studying of $REFe_{1-x}Cr_xO_3$ compounds for a Cr constant concentration by varying the RE ions. Hence, in the present study, to fill this research gap we synthesized and characterized $REFe_{0.7}Cr_{0.3}O_3$ (RE= La, Pr, Nd, Sm, and Gd) nanoparticles (NPs). In our previous study, we investigated the physical properties of $REFeO_3$ NPs that were prepared by similar technique [10]. Therefore, this current work is not only a report on the physical properties of $REFe_{0.7}Cr_{0.3}O_3$ NPs but also compares some results of previous work with the present study. These findings can provide a deep insight into the effects of substitution of Cr ions in light members of rare-earth orthoferrites and propose a new way for optimizing the multifunctional properties of these materials for advanced applications.

2. Experimental method

In this study, $REFe_{0.7}Cr_{0.3}O_3$ powders were synthesized via the sol-gel method. The sol-gel method was chosen because it is cost-effective, simple, allows control over nanoparticle size and homogeneity, and enables the production of high-purity materials under relatively mild conditions [32, 33]. The precursors, $RE(NO_3)_3.xH_2O$, 99.9%, Sigma-Aldrich, $Cr(NO_3)_3.3H_2O$, 99%, Sigma-Aldrich, and $Fe(NO_3)_3.9H_2O$, 99.95%, Merck, in stoichiometric amounts were separately dissolved in deionized water at room temperature (RT), using a magnetic stirrer. Subsequently, an appropriate amount of citric acid ($C_6H_8O_7$, ≥99.5%, Merck) as a chelating agent was added to the precursor solution. Next, the solution was stirred for 2 h, and then the pH of the solution was adjusted to 7 with the help of ammonia solution. The resulting solution was heated at 80 °C for several hours until a brown gel was formed. After that, the resulting gel was pre-heated in air at 400 °C for 4 h, and finally the prepared powders were calcined in air at 900 °C for 2 h.

The crystal structure of $REFe_{0.7}Cr_{0.3}O_3$ powders was examined using an X-ray diffraction instrument (Bruker D8, Germany) with Cu-Kα radiation (λ=1.542 Å) in the 2θ range of 15-75° with a step size of 0.04°/s at RT. The morphology of all samples was investigated using field-emission scanning electron microscopy (FESEM). To confirm the presence of the rare earth elements (La, Pr, Nd, Sm, Gd), Fe, Cr, and O in the synthesized powders, energy dispersive X-ray spectroscopy (EDX) was employed. The magnetic hysteresis loops of all samples were measured by a vibrating sample magnetometer (VSM) (LakeShore Model: 7407) under the applied magnetic fields up to ±20 kOe at RT. The electrical properties of the disk-shaped samples with a diameter of 10 mm and a thickness of 1.0 mm were investigated using an LCR meter (GW Instek 8110G) in two protocols: (1) in the frequency range of 70 to 10^7 Hz at RT, and (2) at the temperature range of 27-250 °C at constant frequency.

3. Results and Discussion

3.1. Structural analysis

X-ray diffraction (XRD) patterns of the $REFe_{0.7}Cr_{0.3}O_3$ (RE= La, Pr, Nd, Sm, and Gd) polycrystalline nanoparticles (NPs) are shown in Figure 1. In the first step, the phase formation of all samples in the orthoferrite structure was investigated using the X'pert software. Results indicate that all prepared NPs have orthorhombic symmetry without any impurity phases. Due to the reduction in the ionic radius of the RE ions with increasing atomic number, a slight shift in the position of the main peak to higher diffraction angles occurs from La to Gd as observed in the inset of Figure 1. This result is in agreement with a previous report on $REFeO_3$ NPs [11]. The Rietveld refinement of the XRD pattern of the $REFe_{0.7}Cr_{0.3}O_3$ NPs is displayed in Figure 2. Appropriate fitting between experimental and simulated data indicates that all samples crystallize in the orthorhombic structure with the *Pbnm* space group. Results of lattice parameters (*a*, *b*, and *c*) and the unit cell volume (*V*) of studied samples compared with those of the $REFeO_3$ light rare earth compounds (based on our previous report [11]) are given in Table 1. Introducing Cr ion into the Fe-site results in a decrease in the unit cell volume between 0.16% - 0.41%. This result is consistent with the fact that the ionic radius of Fe^{3+} is larger than that of Cr^{3+} [34]. A similar trend was also observed in some previous reports [23, 29, 31]. On the other hand, similar to $REFeO_3$ and $REVO_3$ compounds, while *a* and *c* decrease with decreasing RE ionic radius (r_{RE}), *b* increases [7, 8, 35]. Moreover, due to the reduction of r_{RE} from La to Gd, *V* in the studied samples decreases from $LaFe_{0.7}Cr_{0.3}O_3$ to the $GdFe_{0.7}Cr_{0.3}O_3$. Furthermore, the orthorhombic strain, $s = [2(b-a)/(b+a)]$, and tolerance factor, $\tau = [\frac{<RE-O>}{\sqrt{2}(Fe/Cr-O)}]$, that refer to the relative deformation of orthorhombic structure and the criterion of distortion, respectively, which were plotted for $REFe_{0.7}Cr_{0.3}O_3$ compounds in Figure 3a. In the τ relation, <RE-O> and <Fe/Cr-O> are the average of RE-O and Fe/Cr-O bond lengths that are the consequence of Rietveld refinement output for the studied samples. Finally, the variation of <Fe/Cr-O> and $<\varphi> = [(180^0-<Fe/Cr-O-Cr/Fe>_{av})/2]$ versus r_{RE} was drawn in Figure 3b. The similar trend between *s* and <Fe/Cr-O>, and $<\varphi>$ implies that tilting and distortion can affect lattice parameters. Such

behavior was observed in $REFeO_3$ and $REVO_3$ compounds previously [7, 8, 35].

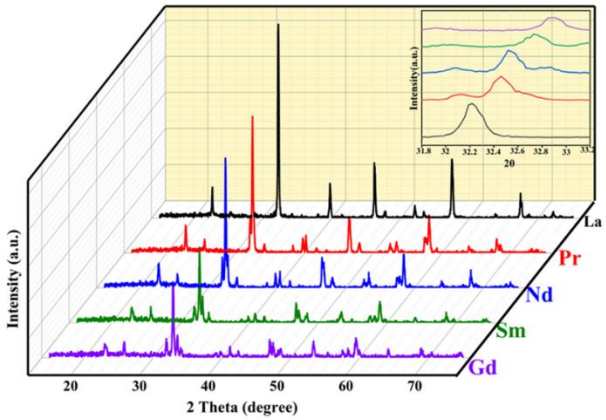

Fig. 1. The XRD pattern for all prepared nanoparticles. Inset shows a shift in the main peak of XRD patterns.

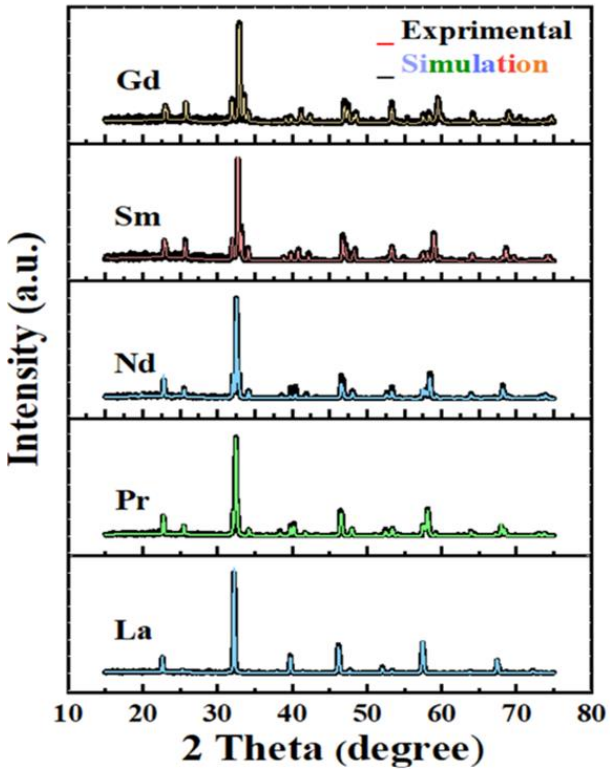

Fig. 2. The Rietveld refinement of XRD patterns for all samples.

The Scherrer equation, $D_{Scherr}=K\lambda/(\beta\cos\theta)$, is a way to evaluate crystallite size in polycrystalline samples. In this relation, K, *λ, θ, and β* correspond to the Scherrer constant, the X-ray wavelength ($Cu_{k\alpha}$=1.542Å), the diffraction angle of the major peak, and the peak broadening of the major peak, respectively. Generally, β depends not only on the crystallite size, but also on the lattice strain (ε). Hence, the crystallite size was also evaluated by another method using the Williamson-Hall equation, $\beta\cos\theta = 4\varepsilon\sin\theta + k\lambda/D_{W\text{-}H}$. To determine $D_{W\text{-}H}$, $\beta\cos\theta$ is plotted versus $4\sin\theta$, as shown in Figure 4. The results of D_{Scherr}, $D_{W\text{-}H}$, and ε are listed in Table 2. The type of strain in the samples determined from the slope of the W-H plots, indicated that the lattice experienced tensile strain.

3.2. Microstructural analysis

To verify the morphology and particle size of the synthesized powders, the FE-SEM technique was used. The FE-SEM photographs shown in Figure 5 display that the prepared $REFe_{0.7}Cr_{0.3}O_3$ NPs are predominantly spherical or ellipsoidal in shape. Due to a clear distinction between grain and grain boundaries, Digimizer software was used to determine the particle size and plot the data as histogram curves (insets of Fig. 5). To estimate the mean particle diameter ($\langle D\rangle_{SEM}$) of $REFe_{0.7}Cr_{0.3}O_3$ NPs, the histogram curve of each sample was well fitted using a log-normal function as [36]:

$$P(D) = (1/\sqrt{2\pi\sigma D})\exp\left[-\ln^2(D/D_0)/2\sigma^2\right] \quad (1)$$

where σ and D_0 are the distribution width and median diameter, respectively. To calculate $\langle D\rangle_{SEM}$ and_standard deviation (σ_D), we put extracted σ and D_0 data from the fitting process into the following relations:

$$< D >_{SEM} = D_0 \exp(\sigma^2/2) \quad (2)$$

$$\sigma_D = < D >_{SEM} [\exp(\sigma^2) - 1]^{1/2} \quad (3)$$

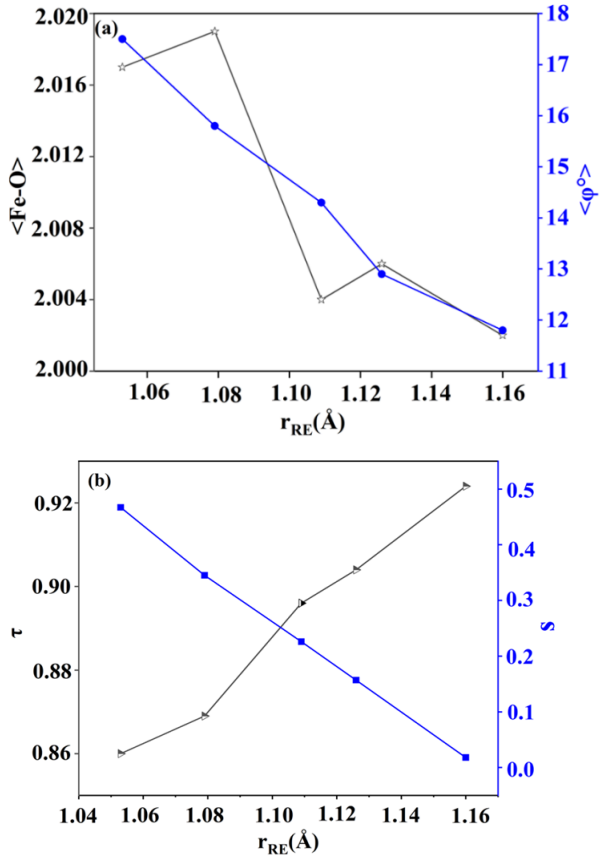

Fig. 3. (a) The average bond length and lattice distortion angle, (b) The orthorhombic strain and tolerance factor, as a function of the ionic radius of RE ions.

All calculated data were given in Table 2. Comparing $\langle D\rangle_{SEM}$ with D_{Scher} / $D_{w\text{-}H}$, it can be concluded that the mean particle diameter is larger than the crystallite size. Finally, using the EDX spectrum of the $REFe_{0.7}Cr_{0.3}O_3$ samples that are revealed presented in Figure 6a, the presence of RE (La, Pr, Nd, Sm, and Gd), Fe, Cr, and O elements is confirmed in the studied compounds. The characteristic peaks of these

elements were used to generate pie charts of their atomic percentages for each compound (Fig. 6b).

3.3. Magnetic analysis

Fig. 7a shows isothermal magnetic hysteresis loops (*M-H* curves) of the $REFe_{0.7}Cr_{0.3}O_3$ compounds under applied magnetic fields up to 20 kOe at RT. All samples exhibit an antiferromagnetic (AFM) nature. However, as seen in Figure 7b, all samples display WFM behavior with low remanent magnetization (M_r) and coercivity field (H_c) values (see Table 3) in comparison to our previous study on $REFeO_3$ samples that were synthesized with a similar method [10]. This result is in good agreement with the literature [37, 38]. Generally, there are two kinds of interactions in $REFeO_3$, $RECrO_3$, and $RE(Fe/Cr)O_3$ compounds, symmetric and antisymmetric. The symmetric one includes RE-O-RE, RE-O-Fe/Cr, and Fe/Cr-O-Cr/Fe components, while the latest one is the most dominant compared to other cases at RT [11, 34, 39]. Based on G-K rules, among Fe^{3+}-O-Fe^{3+}, Cr^{3+}-O-Cr^{3+}, and Fe^{3+}-O-Cr^{3+}exchange interactions, the first two interactions have AFM nature behavior, while the latter one may exhibit ferromagnetic (FM) behavior depending on Fe^{3+}-O-Cr^{3+} bond angle [40, 41]. According to refs of [40] and [41], the Fe^{3+}-O-Cr^{3+} interaction is AFM when the bond angles are below 150˚ and 156˚, respectively. Structural analysis indicates that the Fe/Cr–O–Fe/Cr bond angles in the studied samples lie in the range of 148.5°–157° (Fig. 4a). Therefore, all Fe/Cr-O-Cr/Fe components have an AFM behavior in our compounds. On the other hand, the asymmetric one is the DM interaction that is responsible for the canted magnetic moment of Fe^{3+} and Cr^{3+} and results in the WFM feature in these compounds [38]. Previous report on $SmFe/CrO_3$ displays that the strength of DM interaction increases with increasing Cr content [42]. Therefore, it can be expected that the WFM behavior on our compounds is enhanced by Cr doping compared to $ReFeO_3$ samples. But, this expectation disagrees with the reduction of M_r and H_c values in the current studied samples. This result may be attributed to the decreasing resultant magnetic moment due to the lower magnetic moment of the Cr^{3+} ion (3 μ_B) compared to that of the Fe^{3+} ion (5 μ_B). Furthermore, in order to estimate the strength of Fe/Cr-O-Fe/Cr interaction upon Cr substitution, we determine the Néel transition temperature (T_N) in the studied samples. For instance, Figure 8 shows the temperature dependence of magnetization for samples with R= La at a 1000 Oe applied magnetic field. The T_N is obtained at the temperature at which the dM/dT curve is the minimum. The T_N for all studied samples was listed in Table 3. As observed from Table 3, the T_N for $REFe_{0.7}Cr_{0.3}O_3$ samples decreases with the reduction of r_{RE}. This result is similar to that of $REFeO_3$ compounds [39, 40]. Moreover, T_N in studied compounds declines by Cr substitution in comparison with $REFeO_3$. J.S. Zhou et al. displayed that T_N in the $REFeO_3$ and $RECrO_3$ series correspond closely to the exchange integral (J) between Fe^{3+}/ Cr^{3+} ions, which can be defined as $T_N = 4S(S+1)\ J/k_B$, where S= 5/2 and 3/2 represent the spin of Fe^{3+} and Cr^{3+} ions, respectively [43,44]. The J dependence on the parameters of orbital overlap i.e. φ (defined in structural analysis part) and average Fe/Cr-O bond distance (d) is as $J \propto \cos^4(\varphi)/d^7$ [41-43]. Figure 9 shows the variation of $(\cos^4(\varphi)/d^7)$ (based on structural information corresponding to Fig. 4a) and T_N values versus r_{RE}. It is obvious that the slope of both of them is almost equal. It implies that the strength of super exchange interaction decreases with decreasing r_{RE} due to the reduction of orbitals overlap in $REFe_{0.7}Cr_{0.3}O_3$ compounds.

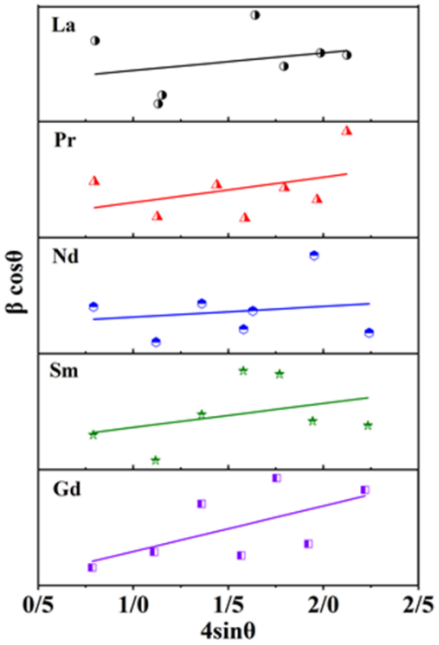

Fig. 4. The W-H plot of $REFe_{0.7}Cr_{0.3}O_3$ samples.

3.4. Dielectric analysis

Fig. 10 (a,b) shows the variation of the real dielectric constant (ε) and dielectric loss ($\tan\delta$) versus frequency for the studied compounds in the frequency range of 70-10^7 Hz at RT. The ε curve for all samples exhibits a significant decrease in the frequency range of 70-10^3 Hz, and then it becomes nearly constant. The considerable value of ε in the low frequency (LF) region is due to space-charge polarization [17]. In fact, as the frequency increases, space-charge carriers can no longer respond to the applied electric field, and the space-charge polarization becomes frozen [37, 45, 46]. As the ionic radius of RE ions increases, there is a corresponding rise in the ε. This phenomenon results in the observation of a colossal dielectric constant (CDC) within the $LaFe_{0.7}Cr_{0.3}O_3$ composition. The CDC behavior is explained by the Maxwell-Wagner (MW) polarization model, which is in agreement with Koop's theory [47]. The significant scattering observed in $REFe_{0.7}Cr_{0.3}O_3$ NPs can be attributed to: i) the accumulation of charge carriers at grain boundaries with low conductivity, and ii) the effect arising from the distortion of the Fe/CrO_6 octahedral [47]. It is clear from Figure 10b, the

dielectric loss decreases with increasing frequency, becoming constant for $f>10^5$ Hz. Such behavior can be explained by grain and grain-boundary effects and MW polarization [6, 48]. The significant value of tanδ falls within the LF range, due to the accumulation of conductive grains at grain boundaries [47].

Fig.11 reveals the frequency-dependence of ac conductivity (σ_{ac}) of $REFe_{0.7}Cr_{0.3}O_3$ compounds using the relation $\sigma(\omega)= \omega\varepsilon_0\varepsilon\tan\delta$ at RT, where ω and ε_0 are the angular frequency and the vacuum permittivity, respectively [37]. Based on various theoretical models, all samples follow the non-overlapping small polarons mechanism (NSPT) so that conductivity increased with increasing frequency [49]. The conductivity spectrum is composed of two distinct components, the first part, frequency-independent conductivity in the LF region, and the second part, an increase in conductivity with increasing frequency in the high frequency (HF) region [50]. The frequency dependence of conductivity is described by the Jonscher power law, $\sigma(\omega)=\sigma_{DC}+A\omega^n$ [26], where σ_{DC} is the direct current conductivity of samples, and the exponent n ($0 \le n \le 1$) quantifies the degree of interaction between mobile ions and their surrounding lattices. Additionally, A is a constant that signifies the strength of polarizability [50]. The temperature-dependent DC conductivity for all samples (measured between 27 to 250 °C) further confirms their semiconducting nature, as seen in Figure 12. The observed change in the slope of the σ_{DC} (T) curve from the $LaFe_{0.7}Cr_{0.3}O_3$ sample signifies a transition from trapped to mobile extrinsic carriers as the temperature increases [51]. According to Figure13, the Jonscher power exponent n as a function of T falls within the range of $0.35\le n\le 1$ for all samples. In situations where the n parameter is less than 1 ($n<1$), conduction occurs due to the movement of mobile charge carriers between localized sites [52]. With increasing temperature, the value of n rises due to a thermally activated process, which follows the correlated barrier hopping (CBH) model. This model supports the NSPT mechanism.

Table 1. Structural parameters of $REFe_{0.7}Cr_{0.3}O_3$. @ Data for $REFeO_3$ were taken from Ref. 11.

Sample@	a (Å)	b (Å)	c (Å)	V (Å)^3	$\Delta V/V$ (%)	τ	s
$LaFeO_3$	5.556(4)	5.562(3)	7.854(6)	242.7(6)		0.910	0.0010
$LaFe_{0.7}Cr_{0.3}O_3$	5.550(2)	5.560(1)	7.846(3)	242.1(4)	-0.26	0.924	0.0018
$PrFeO_3$	5.483(3)	5.580(0)	7.788(6)	238.3(5)		0.880	0.0175
$PrFe_{0.7}Cr_{0.3}O_3$	5.479(8)	5.566(2)	7.782(2)	237.3(7)	-0.41	0.904	0.0157
$NdFeO_3$	5.452(0)	5.585(0)	7.763(4)	236.3(9)		0.874	0.0241
$NdFe_{0.7}Cr_{0.3}O_3$	5.450(6)	5.575(2)	7.759(6)	235.8(0)	-0.25	0.896	0.0226
$SmFeO_3$	5.399(6)	5.598(3)	7.709(0)	233.0(3)		0.870	0.0361
$SmFe_{0.7}Cr_{0.3}O_3$	5.400(4)	5.590(5)	7.706(0)	232.6(5)	-0.16	0.869	0.0345
$GdFeO_3$	5.349(1)	5.561(4)	7.668(4)	230.1(4)		0.866	0.0388
$GdFe_{0.7}Cr_{0.3}O_3$	5.349(1)	5.601(4)	7.661(7)	229.3(9)	-0.32	0.860	0.0467

Table 2. Crystallite size (D_{scherr} and $D_{W\text{-}H}$), lattice strain (ε), mean particle diameter (D_{SEM}), and standard deviation (σ_D) for all synthesized nanoparticles.

Sample	D_{Scher} (nm)	$D_{W\text{-}H}$ (nm)	ε ($\times10^{-1}$)	D_{SEM} (nm)	σ_D (nm)
$LaFe_{0.7}Cr_{0.3}O_3$	73	78	0.47	95	14.61
$PrFe_{0.7}Cr_{0.3}O_3$	73	76	0.46	145	20.78
$NdFe_{0.7}Cr_{0.3}O_3$	58	63	0.40	125	26.70
$SmFe_{0.7}Cr_{0.3}O_3$	49	54	0.50	83	16.53
$GdFe_{0.7}Cr_{0.3}O_3$	59	63	0.62	75	7.92

Table 3. Magnetic parameters for $REFe_{0.7}Cr_{0.3}O_3$ samples.

Sample	M_r (*10^{-3} emu/g)	H_c (Oe)	T_N (K)
$LaFe_{0.7}Cr_{0.3}O_3$	0.6	50	583
$PrFe_{0.7}Cr_{0.3}O_3$	1.9	150	558
$NdFe_{0.7}Cr_{0.3}O_3$	7.0	225	543
$SmFe_{0.7}Cr_{0.3}O_3$	7.2	300	523
$GdFe_{0.7}Cr_{0.3}O_3$	3.2	25	498

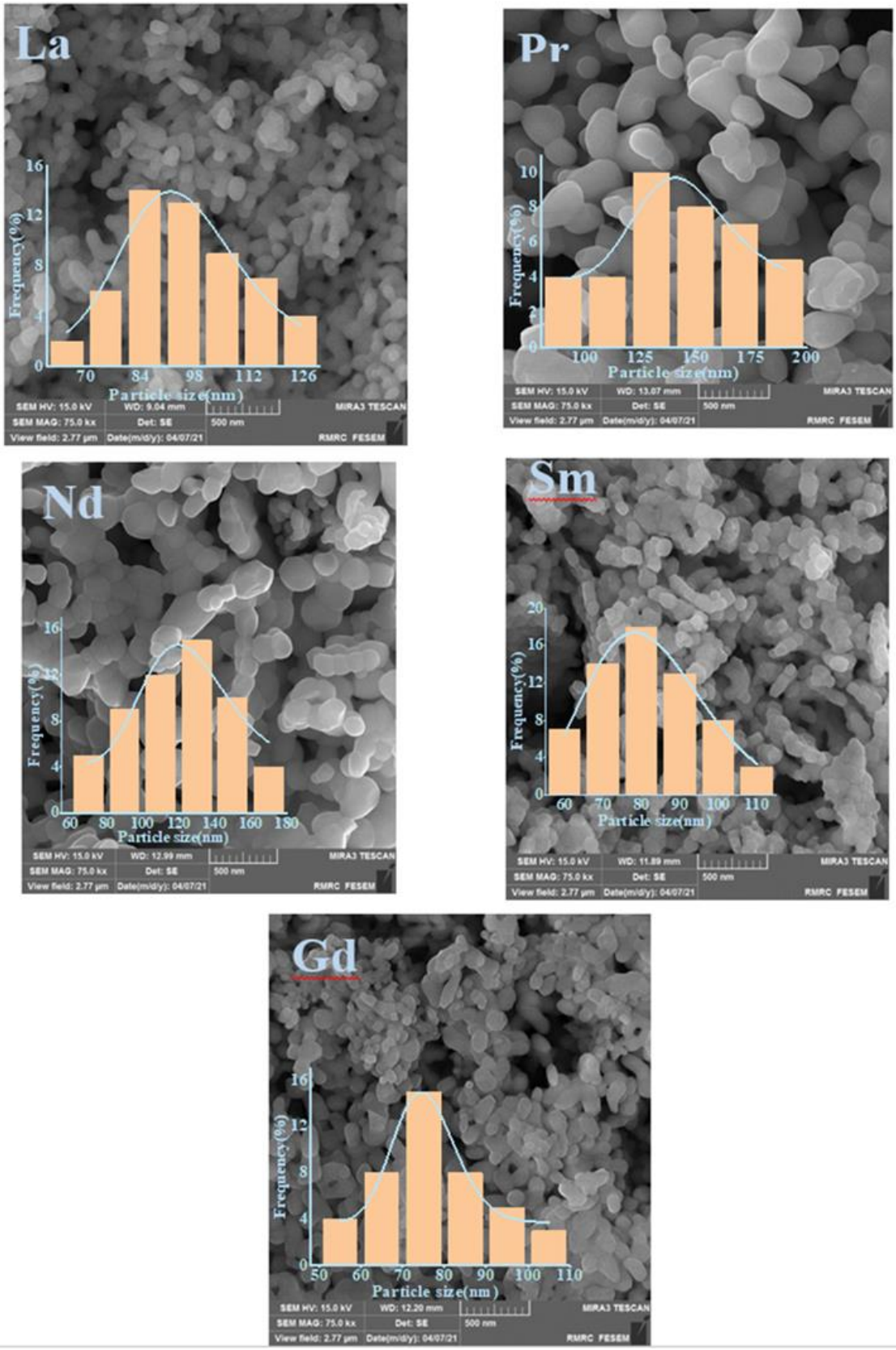

Fig. 5. The FE-SEM image for all synthesized nanoparticles.

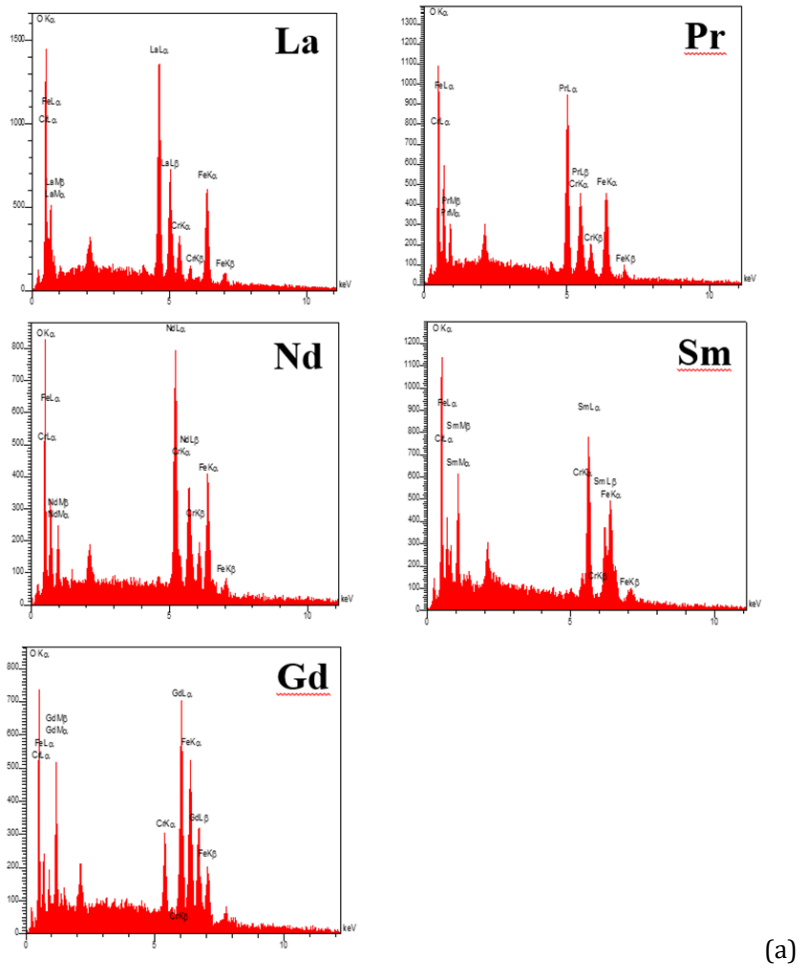

(a)

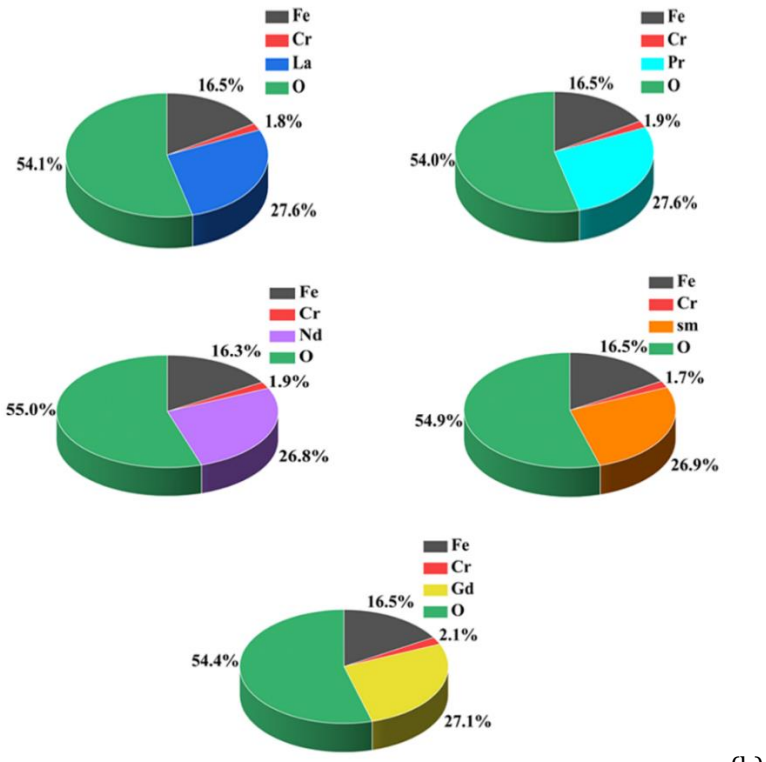

(b)

Fig. 6. (a) EDX spectrum for all samples, (b) the atomic percentage of the constituent elements of each compound.

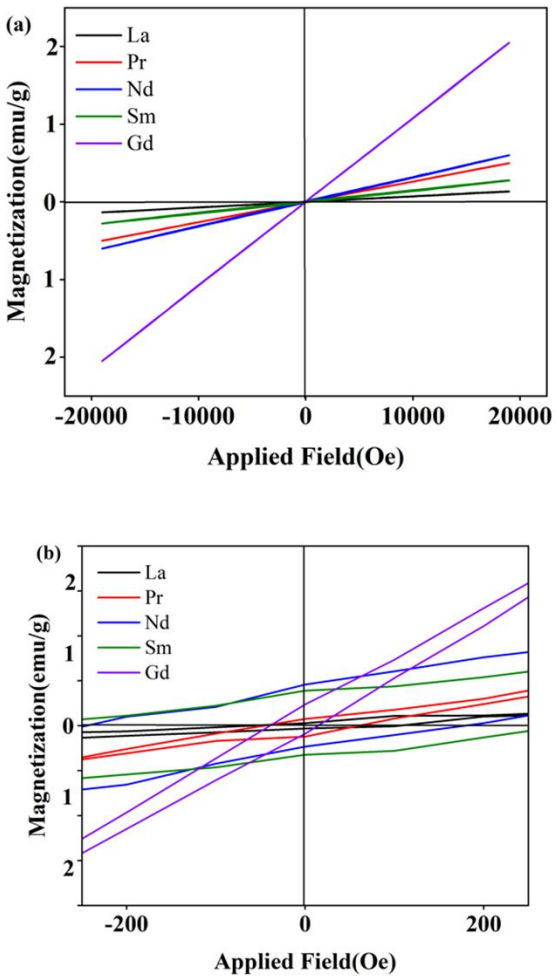

Fig. 7. Isothermal magnetic hysteresis loop of the $REFe_{0.7}Cr_{0.3}O_3$ at RT, (b) Magnification of the magnetic hysteresis loops.

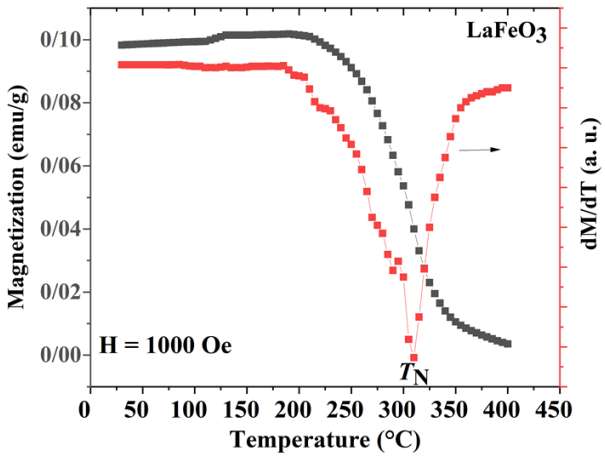

Fig. 8. The temperature dependence of magnetization for a sample with RE= La at 1000 Oe applied magnetic field.

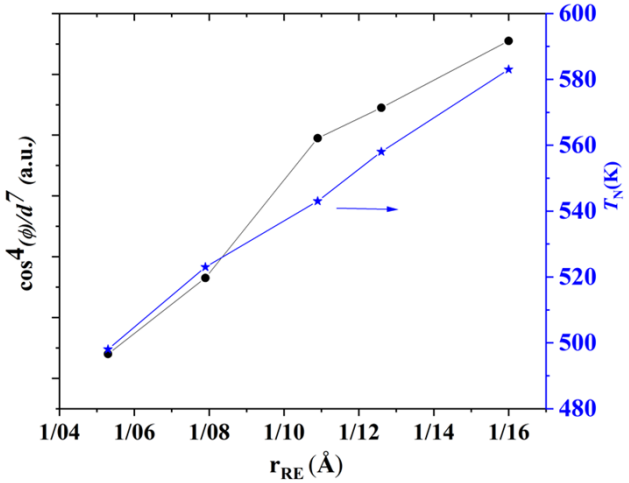

Fig. 9. The variation of ($cos^4(\varphi)/d^7$) and T_N values versus r_{RE}.

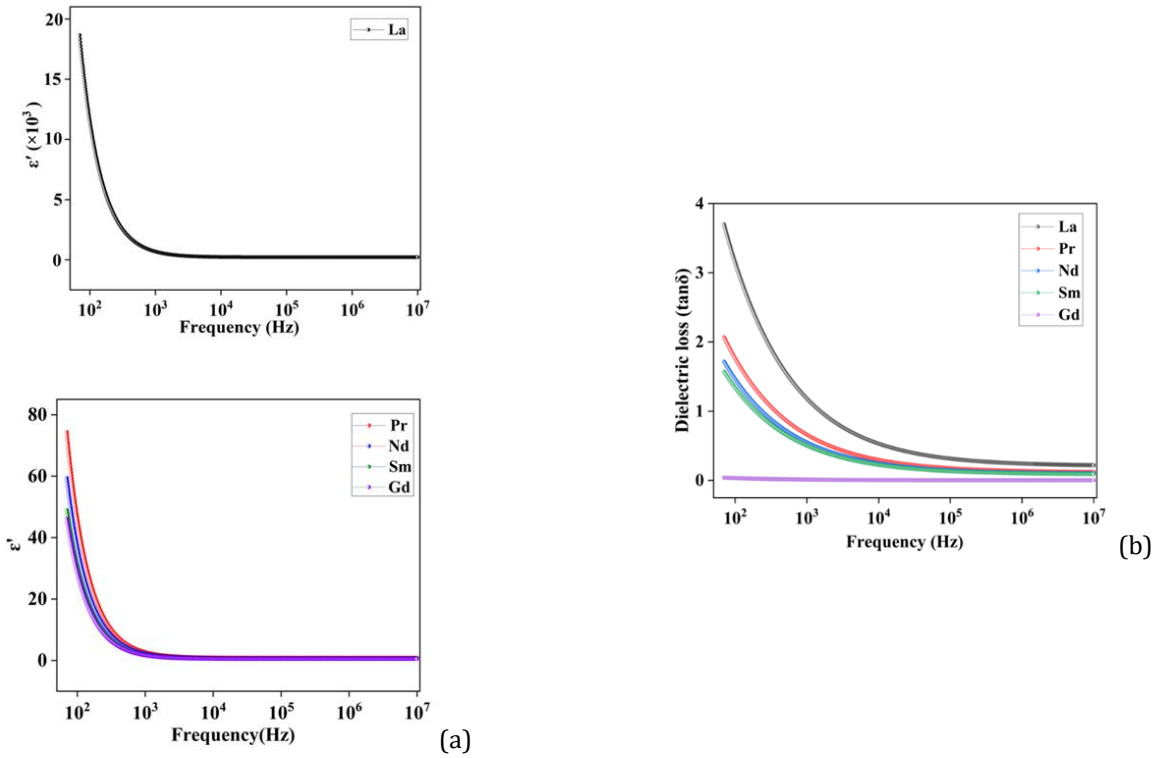

Fig. 10. Frequency dependence of (a) the real dielectric components ε, (b) the loss dielectric $tan\delta$, for the $REFe_{0.7}Cr_{0.3}O_3$ at RT.

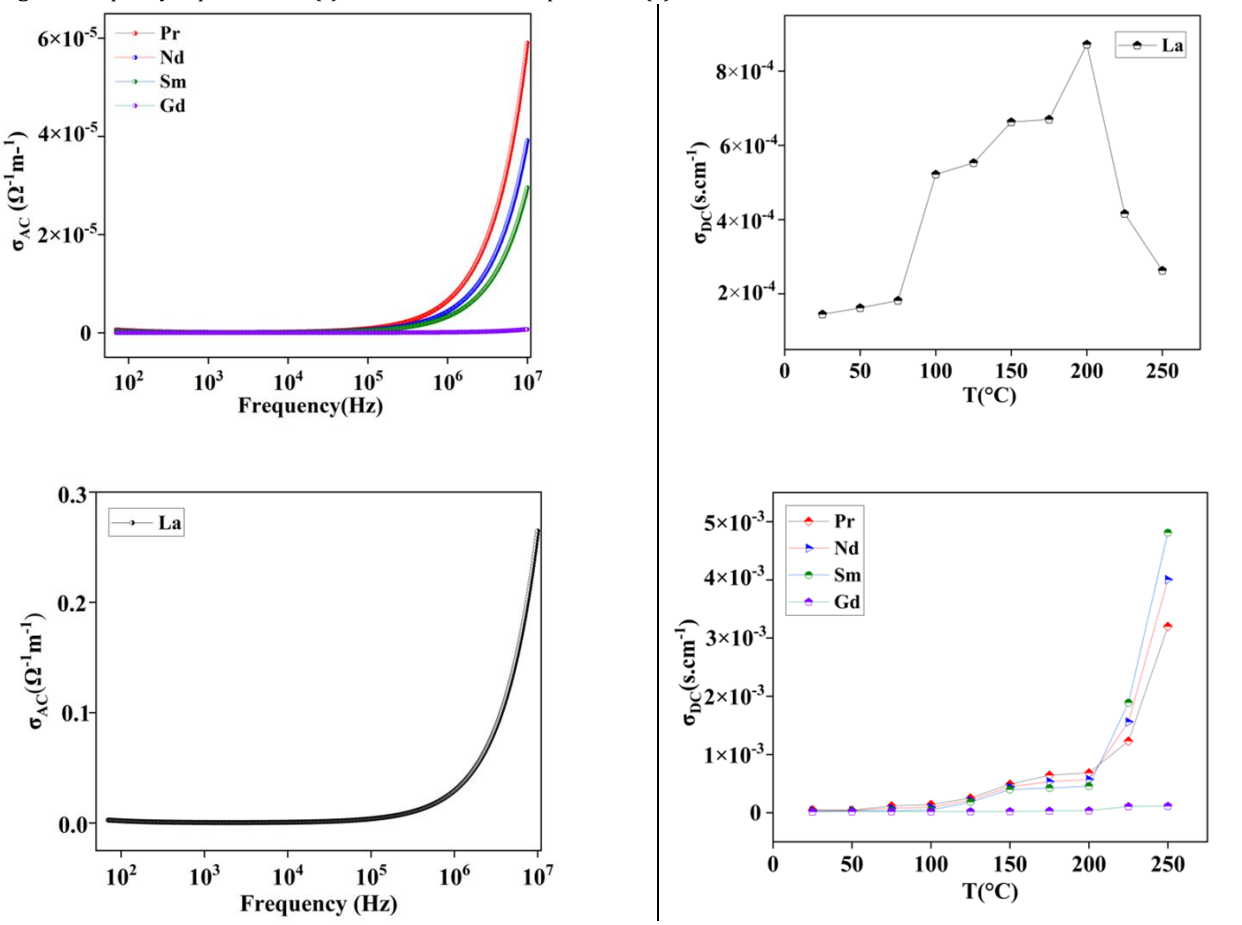

Fig. 11. The frequency dependence of ac conductivity (σ_{ac}) for $REFe_{0.7}Cr_{0.3}O_3$ at RT.

Fig. 12 The temperature dependence of DC conductivity (σ_{Dc}) for $REvaFe_{0.7}Cr_{0.3}O_3$.

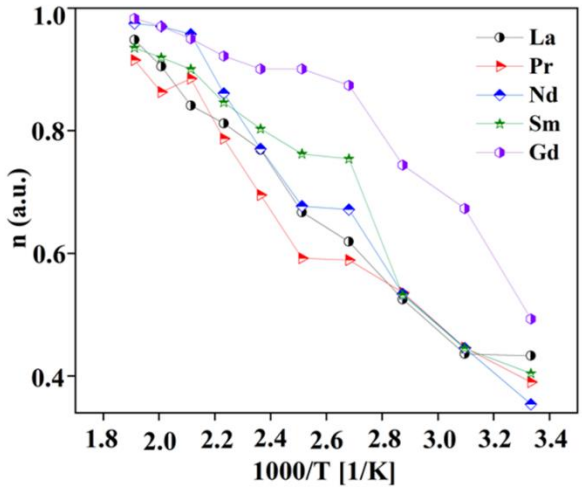

Fig. 13. The temperature dependence of exponent *n*, for $REFe_{0.7}Cr_{0.3}O_3$.

4. Conclusions

In the present study, we have carried out a detailed investigation of structural, magnetic, and electrical properties of $REFe_{0.7}Cr_{0.3}O_3$ (RE= La, Pr, Nd, Sm, and Gd) perovskite oxides. The XRD analysis confirms that all samples are single phase with orthorhombic symmetry. Owing to the reduction of r_{RE} from La to Gd, the unit cell volume in the prepared samples decreases from $LaFe_{0.7}Cr_{0.3}O_3$ to $GdFe_{0.7}Cr_{0.3}O_3$. Similar to undoped orthoferrites, tilting and distortion increase with the reduction of r_{RE} from La to Gd. All samples reveal a WFM behavior. $REFe_{0.7}Cr_{0.3}O_3$ compounds undergo a magnetic phase transition from the AFM phase to the paramagnetic phase, so that the Néel transition temperature decreases with decreasing r_{RE}. The dielectric measurements confirm that the $LaFe_{0.7}Cr_{0.3}O_3$ sample shows a CDC feature. Owing to this high dielectric constant and low dielectric loss, we conclude that these materials can be effectively utilized in miniaturized electronic components, high-dielectric capacitors, and memory/storage devices. Based on various theoretical models, all samples follow the non-overlapping small polaron mechanism.

Funding Statement

This research received no specific grant from any funding agency.

Conflicts of interest

The authors declare that they have no known competing financial interests or personal relationships that could have appeared to influence the work reported in this paper.

Authors contribution statement

Roksana Haji: Data analysis and experimentation, Manuscript writing and editing, Data analysis and interpretation. **Davoud Sanavi Khoshnoud**: Conceptualization and study design, Manuscript writing and editing, Data analysis and interpretation, Supervision and project administration.

References

[1] Pecovska-Gjorgjevich, M., Aleksovska, S., Dimitrovska-Lazova, S. and Marinšek, M., 2016. The role of Cr/Co substitution on dielectric properties of gadolinium orthochromite. *Physica Scripta*, *91*(4), p.045805.

[2] Li, K., Wang, D., Wu, F., Xie, T. and Li, T., 2000. Surface electronic states and photovoltage gas-sensitive characters of nanocrystalline $LaFeO_3$. *Materials chemistry and physics*, *64*(3), pp.269-272.

[3] Li, X., Tang, C., Ai, M., Dong, L. and Xu, Z., 2010. Controllable synthesis of pure-phase rare-earth orthoferrites hollow spheres with a porous shell and their catalytic performance for the CO^+ NO reaction. *Chemistry of Materials*, *22*(17), pp.4879-4889.

[4] Arabi, A., Fazli, M. and Ehsani, M.H., 2022. Photocatalytic activity of the $La0.7Ca_{0.3}MnO_3$ nanorods. *Progress in Physics of Applied Materials*, *2*(2), pp.123-131.

[5] Jeong, Y.K., Lee, J.H., Ahn, S.J. and Jang, H.M., 2012. Temperature-induced magnetization reversal and ultra-fast magnetic switch at low field in $SmFeO_3$. *Solid state communications*, *152*(13), pp.1112-1115.

[6] Ahmad, I., Akhtar, M.J., Younas, M., Siddique, M. and Hasan, M.M., 2012. Small polaronic hole hopping mechanism and Maxwell-Wagner relaxation in $NdFeO_3$. *Journal of Applied Physics*, *112*(7).

[7] Wang, Z.Q., Lan, Y.S., Zeng, Z.Y., Chen, X.R. and Chen, Q.F., 2019. Magnetic structures and optical properties of rare-earth orthoferrites $RFeO_3$ (R= Ho, Er, Tm and Lu). *Solid State Communications*, *288*, pp.10-17.

[8] Kamal Warshi, M., Mishra, V., Sagdeo, A., Mishra, V., Kumar, R. and Sagdeo, P.R., 2018. Synthesis and characterization of $RFeO_3$: experimental results and theoretical prediction. *Advances in Materials and Processing Technologies*, *4*(4), pp.558-572.

[9] Lee, J.H., Jeong, Y.K., Park, J.H., Oak, M.A., Jang, H.M., Son, J.Y. and Scott, J.F., 2011. Spin-Canting-Induced Improper Ferroelectricity and Spontaneous Magnetization Reversal in $SmFeO_3$. *Physical review letters*, *107*(11), p.117201.

[10] Nakhaei, M. and Khoshnoud, D.S., 2019. Influence of particle size and lattice distortion on magnetic and

dielectric properties of $NdFeO_3$ orthoferrite. *Physica B: Condensed Matter*, *553*, pp.53-58.

[11] Nakhaei, M. and Khoshnoud, D.S., 2021. Structural, magnetic, and electrical properties of $RFeO_3$ (R= Dy, Ho, Yb & Lu) compounds. *Journal of Materials Science: Materials in Electronics*, *32*(11), pp.14286-14300.

[12] Nakhaei, M. and Khoshnoud, D.S., 2021. Study on structural, magnetic and electrical properties of $ReFeO_3$ (Re= La, Pr, Nd, Sm & Gd) orthoferrites. *Physica B: Condensed Matter*, *612*, p.412899.

[13] Dehno, R.T. and Khoshnoud, D.S., 2022. Multiferroic properties in Sm1-xErxFeO_3 ceramics. *Journal of Magnetism and Magnetic Materials*, *541*, p.168515.

[14] Ghasemi, E. and Khoshnoud, D.S., 2025. The effect of Mg doping on spin reorientation transition and physical properties of $SmFeO_3$. *Journal of Materials Science: Materials in Electronics*, *36*(5), p.304.

[15] Kashyap, S.J., Sankannavar, R. and Madhu, G.M., 2022. Insights on the various structural, optical and dielectric characteristics of $La_{1-x}ca_xFeO_3$ perovskite-type oxides synthesized through solution-combustion technique. *Applied Physics A*, *128*(6), p.518.

[16] Huang, L., Cheng, L., Pan, S., Yao, Q., Long, Q., Wang, M., Chen, Y. and Zhou, H., 2022. Influence of A-site doping barium on structure, magnetic and microwave absorption properties of $LaFeO_3$ ceramics powders. *Journal of Rare Earths*, *40*(7), pp.1106-1117.

[17] Makoed, I.I., Liedienov, N.A., Pashchenko, A.V., Levchenko, G.G., Tatarchuk, D.D., Didenko, Y.V., Amirov, A.A., Rimski, G.S. and Yanushkevich, K.I., 2020. Influence of rare-earth doping on the structural and dielectric properties of orthoferrite $La_{0.5}0R_{0.5}0FeO_3$ ceramics synthesized under high pressure. *Journal of Alloys and Compounds*, *842*, p.155859.

[18] Ruffo, A., Mozzati, M.C., Albini, B., Galinetto, P. and Bini, M., 2020. Role of non-magnetic dopants (Ca, Mg) in $GdFeO_3$ perovskite nanoparticles obtained by different synthetic methods: structural, morphological and magnetic properties. *Journal of Materials Science: Materials in Electronics*, *31*(20), pp.18263-18277..

[19] Tufiq Jamil, M., Ahmad, J., Hamad Bukhari, S. and Saleem, M., 2018. Effect of Re and Tm-site on morphology structure and optical band gap of $ReTmO_3$ (Re= La, Ce Nd, Gd, Dy, Y and Tm= Fe, Cr) prepared by sol-gel method. *Revista mexicana de física*, *64*(4), pp.381-391.

[20] Shanker, J., Venkataramana, K., Prasad, B.V., Kumar, R.V. and Babu, D.S., 2018. Influence of Fe substitution on structural and electrical properties of Gd orthochromite ceramics. *Journal of Alloys and Compounds*, *732*, pp.314-327.

[21] Somvanshi, A., Husain, S. and Khan, W., 2019. Investigation of structure and physical properties of cobalt doped nano-crystalline neodymium orthoferrite. *Journal of Alloys and Compounds*, *778*, pp.439-451.

[22] Orlinski, K., Diduszko, R., Kopcewicz, M. and Pawlak, D.A., 2017. The influence of chromium substitution on crystal structure and shift of Néel transition in $GdFe_{1-x}Cr_xO_3$ mixed oxides. *Journal of Thermal Analysis and Calorimetry*, *127*(1), pp.181-187.

[23] Nithya, V.D., Immanuel, R.J., Senthilkumar, S.T., Sanjeeviraja, C., Perelshtein, I., Zitoun, D. and Selvan, R.K., 2012. Studies on the structural, electrical and magnetic properties of $LaCrO_3$, $LaCr_{0.5}Cu_{0.5}O_3$ and $LaCr_{0.5}Fe_{0.5}O_3$ by sol–gel method. *Materials Research Bulletin*, *47*(8), pp.1861-1868.

[24] Nforna, E.A., Tsobnang, P.K., Fomekong, R.L., Tedjieukeng, H.M.K., Lambi, J.N. and Ghogomu, J.N., 2021. Effect of B-site Co substitution on the structure and magnetic properties of nanocrystalline neodymium orthoferrite synthesized by auto-combustion. *Royal Society Open Science*, *8*(2), p.201883.

[25] Selvadurai, A.P.B., Pazhanivelu, V., Jagadeeshwaran, C., Murugaraj, R., Muthuselvam, I.P. and Chou, F.C., 2015. Influence of Cr substitution on structural, magnetic and electrical conductivity spectra of $LaFeO_3$. *Journal of Alloys and Compounds*, *646*, pp.924-931.

[26] Suthar, L., Bhadala, F., Kumari, P., Mishra, S.K. and Roy, M., 2021. Effect of Mn substitution on crystal structure and electrical behaviour of $YFeO_3$ ceramic. *Ceramics International*, *47*(13), pp.19007-19018.

[27] Mguedla, R., Kharrat, A.B.J., Saadi, M., Khirouni, K., Chniba-Boudjada, N. and Boujelben, W., 2020. Structural, electrical, dielectric and optical properties of $PrCrO_3$ ortho-chromite. *Journal of Alloys and Compounds*, *812*, p.152130.

[28] Sharma, M.K., Basu, T., Mukherjee, K. and Sampathkumaran, E.V., 2016. Effect of rare-earth (Er and Gd) substitution on the magnetic and multiferroic properties of $DyFe_{0.5}Cr_{0.5}O_3$. *Journal of Physics: Condensed Matter*, *28*(42), p.426003.

[29] Kotnana, G., 2018. Magnetic properties and their correlation with lattice dynamics in $HoFe_{1-x}CrxO_3$ ($0 \leq x \leq 1$) compounds *(Doctoral dissertation, Indian Institute of Technology Hyderabad).*

[30] Shanker, J., Prasad, B.V., Suresh, M.B., Kumar, R.V. and Babu, D.S., 2017. Electrical properties of $NdCr_{1-x}FexO_3$ perovskite ceramic nanoparticles—An impedance spectroscopy studies. *Materials Research Bulletin*, *94*, pp.385-398.

[31] Singh, D., Gupta, S. and Mahajan, A., 2016. Structural and composition dependent transport properties of perovskite oxides $La_{0.8}R_{0.2}Fe_{0.5}Cr_{0.5}O_3$ (R= La, Nd, Gd and Dy). *Ceramics International*, *42*(9), pp.11020-11024.

[32] Gholizadeh, A. and Hosseini, S., 2026. Structural and Magnetic Phase Transitions in $Cu_{1-3x}Zn_{2x}Mn_xFe_2O_4$ Ferrites. *Progress in Physics of Applied Materials*, *6*(1), pp.1-13.

[33] Admi, R.I., Kurniawan, B., Saptari, S.A., Yudharma, G. and Munazat, D.R., 2024. Effect of Sintering Temperature on Phase Characteristic and Grain Size of $La_{0.7}AE_{0.3}MnO_3$ (AE= Ba/Ca/Sr) Ceramics Prepared by Sol-Gel Method. *Progress in Physics of Applied Materials*, *4*(1), pp.93-101.

[34] Shannon, R.D., 1976. Revised effective ionic radii and systematic studies of interatomic distances in halides and chalcogenides. *Foundations of Crystallography*, *32*(5), pp.751-767.

[35] Martínez-Lope, M.J., Alonso, J.A., Retuerto, M. and Fernández-Díaz, M.T., 2008. Evolution of the crystal structure of RVO_3 (R= La, Ce, Pr, Nd, Tb, Ho, Er, Tm, Yb,

Lu, Y) perovskites from neutron powder diffraction data. *Inorganic chemistry*, *47*(7), pp.2634-2640.

[36] Rahimkhani, M., Khoshnoud, D.S. and Ehsani, M.H., 2018. Origin of enhanced multiferroic properties in $Bi_{0.85-x}La_{0.15}Ho_xFeO_3$ nanopowders. *Journal of Magnetism and Magnetic Materials*, *449*, pp.538-544.

[37] Mohamed, M.B., Wang, H. and Fuess, H., 2010. Dielectric relaxation and magnetic properties of Cr doped $GaFeO_3$. *Journal of Physics D: Applied Physics*, *43*(45), p.455409.

[38] Bora, T. and Ravi, S., 2013. Study of magnetization reversal in $LaCr_{1-x}Fe_xO_3$ compounds. *Journal of Applied Physics*, *114*(3).

[39] Aparnadevi, N., Saravana Kumar, K., Manikandan, M., Paul Joseph, D. and Venkateswaran, C., 2016. Room temperature dual ferroic behaviour of ball mill synthesized $NdFeO_3$ orthoferrite. *Journal of Applied Physics*, *120*(3).

[40] Bhuyan, M.D.I., Das, S. and Basith, M.A., 2021. Sol-gel synthesized double perovskite Gd_2FeCrO_6 nanoparticles: structural, magnetic and optical properties. *Journal of Alloys and Compounds*, *878*, p.160389.

[41] Moskvin, A.S., Ovanesyan, N.S. and Trukhtanov, V.A., 1975. Angular dependence of the superexchange interactionFe^{3+}-O^{2-}-Cr^{3+}. *Hyperfine Interactions*, *1*(1), pp.265-281.

[42] Xiang, Z., Li, W. and Cui, Y., 2018. Intrinsic structural distortion and exchange interactions in $SmFe_xCr_{1-x}O_3$ compounds. *RSC advances*, *8*(16), pp.8842-8848.

[43] Zhou, J.S., Alonso, J.A., Pomjakushin, V., Goodenough, J.B., Ren, Y., Yan, J.Q. and Cheng, J.G., 2010. Intrinsic structural distortion and superexchange interaction in the orthorhombic rare-earth perovskites $RCrO_3$. *Physical Review B—Condensed Matter and Materials Physics*, *81*(21), p.214115.

[44] Zhou, J.S. and Goodenough, J.B., 2008. Intrinsic structural distortion in orthorhombic perovskite oxides. *Physical Review B—Condensed Matter and Materials Physics*, *77*(13), p.132104.

[45] Jonscher, A.K., 1999. Dielectric relaxation in solids. *Journal of Physics D: Applied Physics*, *32*(14), p.R57.

[46] Zriouil, M., Lahmar, A., Antic-Fidancev, E., Ashehoug, P., Fukami, T. and Elouadi, B., 2008. STRUCTURE, DIELECTRIC AND SPECTROSCOPIC INVESTIGATION OF $(Sr_{1-x}Na_x)$ 0.8 $(K_{1-x}Ln_x)$ 0.4Nb2O6 WITH (Ln= Nd, Eu). *Physical & chemical news*, (44), pp.96-102.

[47] Shanker, J., Suresh, M.B., Saravanan, P. and Babu, D.S., 2019. Effects of Fe substitution on structural, electrical and magnetic properties of erbium ortho-chromite nano polycrystalline material. *Journal of Magnetism and Magnetic Materials*, *477*, pp.167-181.

[48] Huang, S., Shi, L., Tian, Z., Yuan, S., Wang, L., Gong, G., Yin, C. and Zerihun, G., 2015. High-temperature colossal dielectric response in $RFeO_3$ (R= La, Pr and Sm) ceramics. *Ceramics International*, *41*(1), pp.691-698.

[49] Megdiche, M., Perrin-Pellegrino, C. and Gargouri, M., 2014. Conduction mechanism study by overlapping large-polaron tunnelling model in $SrNiP_2O_7$ ceramic compound. *Journal of alloys and compounds*, *584*, pp.209-215.

[50] Omri, A., Bejar, M., Dhahri, E., Es-Souni, M., Valente, M.A., Graça, M.P.F. and Costa, L.C., 2012. Electrical conductivity and dielectric analysis of $La_{0.75}(Ca, Sr)_{0.25}Mn_{0.85}Ga_{0.15}O_3$ perovskite compound. *Journal of alloys and compounds*, *536*, pp.173-178.

[51] Ramu, N., Meera, K., Ranjith, R. and Muralidharan, R., 2018. The role of B-site substitution on the structural and dielectric properties of samarium orthoferrite polycrystals. *Materials Research Express*, *6*(3), p.036106.

[52] Dhahri, A., Dhahri, E. and Hlil, E.K., 2018. Electrical conductivity and dielectric behaviour of nanocrystalline $La_{0.6}Gd_{0.1}Sr_{0.3}Mn_{0.7}5Si_{0.25}O_3$. *Rsc Advances*, *8*(17), pp.9103-9111.